Calculations of Signal-To-Noise Ratios For Solar Radar Echoes

by
P. Yoh

Scientific Report No. 2
July 18, 1961

PREPARED UNDER
AIR FORCE CONTRACT AF19(604)-7436

RADIOSCIENCE LABORATORY
STANFORD ELECTRONICS LABORATORIES
STANFORD UNIVERSITY · STANFORD, CALIFORNIA

CALCULATIONS OF SIGNAL-TO-NOISE RATIOS FOR SOLAR RADAR ECHOES

by

P. Yoh

Scientific Report No. 2
July 18, 1961

Prepared under
Air Force Contract AF19(604)-7436

The research reported in this document has been sponsored by
Electronics Research Directorate
Air Force Cambridge Research Laboratories
Office of Aerospace Research
United States Air Force
Bedford, Massachusetts

Radioscience Laboratory
Stanford Electronics Laboratories
Stanford University Stanford, California

Requests for additional copies by Agencies of the Department of Defense, their contractors, and other Government agencies should be directed to the:

ARMED SERVICES TECHNICAL INFORMATION AGENCY
ARLINGTON HALL STATION
ARLINGTON 12, VIRGINIA

Department of Defense contractors must be established for ASTIA services or have their 'need-to-know' certified by the cognizant military agency of their project or contract.

All other persons and organizations should apply to the:

U.S. DEPARTMENT OF COMMERCE
OFFICE OF TECHNICAL SERVICES
WASHINGTON 25, D. C.

SUMMARY

The procedure for computing the signal-to-noise ratio of radar echoes from the sun is outlined in this report. The radial distribution of electron density in the corona, the coronal temperature, solar noise, galactic noise, and radar-system parameters are taken into account. Examples are given of computations for two solar radar systems that will soon be in operation.

TABLE OF CONTENTS

LIST OF ILLUSTRATIONS

I. INTRODUCTION

The first radar contact with the sun [Ref. 1] was made in April 1959. This success marked the beginning of solar radar astronomy, a promising new approach to the study of the solar corona. Some characteristics which may be measured by radar are: (1) the rate of rotation of the corona; (2) the change of the coronal structure with various types of solar activity; (3) the absorption characteristics of the corona; (4) the roughness and mass motion of the corona; (5) the effects of local and general solar magnetic fields. In this report are presented the steps for computing the signal-to-noise ratio of radar echoes from the sun, and examples are given using the parameters of several new solar radar systems. The results give us a rough estimate of the sensitivity of these systems under various conditions, and hence an indication of our ability to measure some of the solar parameters listed above.

II. ASSUMPTIONS AND COMPUTATIONAL PROCEDURE

In the following computations of the radar cross section of the sun, it is assumed that:

1. The corona is a fully ionized region, and its electron density distribution is given by the Allen-Baumbach equation multiplied by a factor n (a numeric):

$$N = n\, 10^{14} \left(1.55\, \rho^{-6} - 2.99\, \rho^{-16}\right) \text{ electrons/m}^3,$$

   where ρ is the radial distance in units of the solar optical radius $R_\odot$ measured from the center of the sun. The range of n is approximately from 0.5 to 10, its value depending on solar activity.

2. The corona is isothermal at assumed electron temperatures from 5×10^5 °K to 3×10^6 °K. This range of temperature is based on solar radio-astronomy observations.

3. The corona is spherically symmetric and has a smooth reflecting

surface (i.e., directivity = 1). Kerr [Ref. 2] suggests a directivity of 4 because of probable roughness of the contours of constant density. A precise evaluation of this effect must await careful radar studies; therefore, the pessimistic assumption of a directivity of 1 will be used here.

4. An average value of the galactic noise is used. Actually, of course, the galactic noise is higher than average toward the center of the galaxy and lower toward the poles.
5. Solar noise is considered under quiet solar conditions.
6. Magnetic-field effects from both the sun and the earth are neglected.
7. Solar and galactic noise is greater than atmospheric and man-made noise in the frequency range from 20 to 60 Mc.

With the above assumptions, the following quantities are computed in the indicated order:

1. Optical depth, τ
2. Central-ray turning point, ρ_o
3. Radar cross section, σ
4. Solar apparent temperature, T_a
5. Echo power intercepted by the receiving antenna, P_r
6. Galactic noise, P_g
7. Solar noise, P_s
8. Band width, Δf
9. Signal-to-noise ratio, S/N.

These quantities are discussed individually below.

A. OPTICAL DEPTH, τ

The optical depth τ along a trajectory S is defined by

$$\tau = \int_o^\infty \kappa \, ds, \qquad (1)$$

[Ref. 3], where κ is the absorption coefficient of the medium in which the ray travels. From the Lorentz theory, we have

$$\kappa = \frac{\nu x}{c\mu}, \qquad \text{nepers/meter} \tag{2}$$

where

c = velocity of light,

μ = refractic index = $[1 - (f_o^2/f^2)]^{1/2}$,

$x = f_o^2/f^2$,

f_o = plasma frequency = $(e^2 N/4\pi^2 \epsilon_o m)^{1/2}$,

f = wave frequency,

e = electron charge,

N = density of electrons,

m = electron mass, and

ν = frequency of collisions of electrons with ions

$$= \frac{4}{3} e^4 \left[\frac{\pi}{2m(kT_e)^3}\right]^{1/2} Z^2 N_i A_1(2), \tag{3}$$

where

k = Boltzmann's constant,

T_e = electron kinetic temperature,

Z = degree of ionization, and

N_i = positive-ion density.

It seems quite adequate for our purpose to assume the solar atmosphere to be fully ionized hydrogen, so that $N_i = N$ and $Z = 1$. $A_1(2)$ is given by

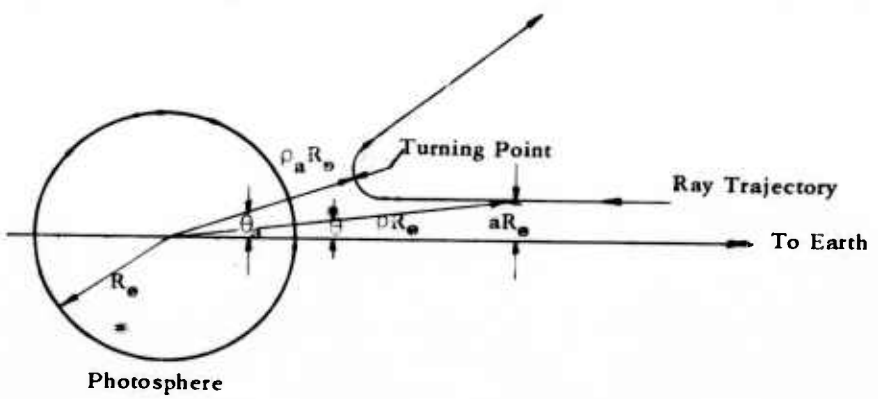

FIG. 1. RAY TRAJECTORY IN THE SOLAR CORONA

$$A_1(2) = \ell n \left[1 + \left(\frac{4\ k\ T_e}{Z\ e^2\ N_i^{1/3}} \right)^2 \right]. \qquad (4)$$

[Ref. 4]. $A_1(2)$ is a slowly varying function of density and temperature, and, to a good degree of approximation, it can be expressed as

$$A_1(2) \approx 2\ \ell n \frac{4\ k\ T_e}{Z\ e^2\ N^{1/3}}$$

$$= 15.567 + 2\ \ell n\ T_e - \frac{2}{3}\ \ell n\ N. \qquad (5)$$

Then Eq. (3) reduces to

$$\nu = \frac{1.816\ N}{T_e^{3/2}}\ A_1(2).$$

The term ds can be expressed as

$$ds = R_\odot\ [(d\rho)^2 + \rho^2 (d\theta)^2]^{1/2} \qquad (6)$$

in polar coordinates whose origin is located at the center of the sun (Fig. 1).

Therefore, Eq. (1) can be written as

$$\tau = \frac{R_\odot}{c} \int_{\rho_a} \frac{\nu x}{\sqrt{\mu^2 - (a^2/\rho^2)}}\ d\rho \qquad (7)$$

and Eq. (7) can be reduced as

$$\tau \begin{pmatrix} Te, n \\ f,\ a \end{pmatrix} = \frac{5.193 \times 10^4\ A_1(2)\ f^2}{T_e^{3/2}}\ I\left(a, \frac{n}{f^2}\right), \qquad (8)$$

[Ref. 5], where $I(a,n/f^2)$ is the integral part of the optical depth. The values of $A_1(2)$ and $I(a, n/f^2)$ have been replotted in Figs. 2 and 3 [Ref. 6].

The method of evaluating the optical depth through the corona is as follows:

1. Choose the wave frequency f (Mc) and a density multiplier n.
2. Form the parameter n/f^2 for the values chosen in item 1.
3. Choose the ray path in terms of a. In our calculation a was chosen for the central ray, i.e., a = 0.
4. Find values of I from Fig. 2 for the selected values of a and n/f^2.
5. Choose an assumed coronal temperature T_e.
6. Determine $A_1(2)$ from the curves in Fig. 3 for the selected values of T_e, n, and f.

With the above procedure, three sets of curves were drawn in Fig. 4, with τ vs f for $T_e = 5 \times 10^5$, 10^6, and 3×10^6 °K and n = 0.5, 1, 2, 5, and 10. Several conclusions are apparent from the curves.

1. As T_e increases, τ decreases, $\tau \propto T_e^{-3/2}$.
2. As n increases, τ increases, $\tau \propto n^{1/4}$
3. As f increases, τ increases, $\tau \propto f^{3/2}$.
4. As a increases, τ decreases.

Result 4 will be shown in later calculations and indicates that the corona is optically thin for large a.

B. TURNING POINT, ρ_o, OF THE CENTRAL RAY

The refractive index μ in a medium containing N free electrons/cubic meter is given by

$$\mu^2 = 1 - \frac{N e^2}{\epsilon_o m(\omega^2 + \nu^2)} \qquad (9)$$

Expressing Eq. (9) in terms of ρ and taking $\omega \gg \nu$, we have

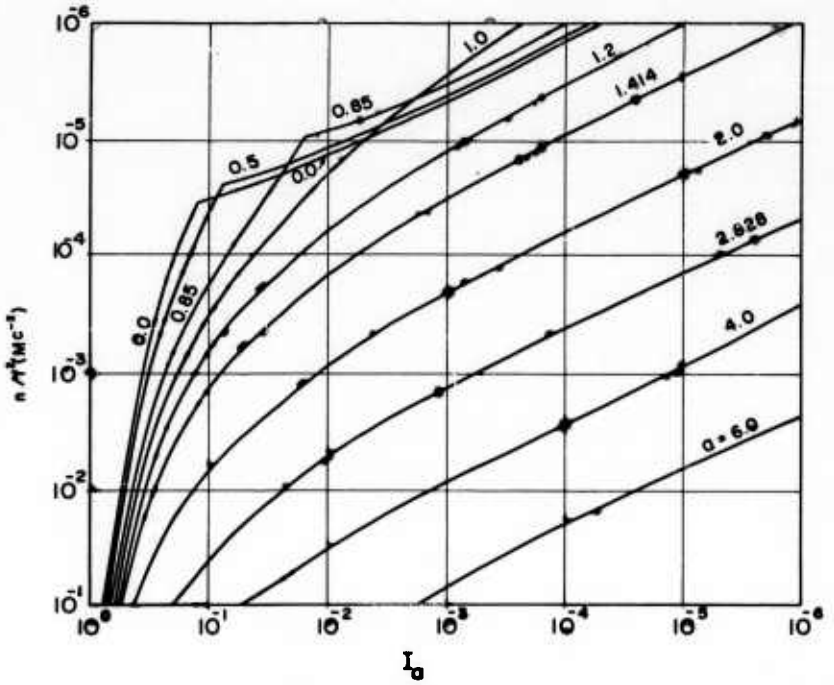

FIG. 2. INTEGRAL PART OF THE EXPRESSION FOR OPTICAL DEPTH (SMERD), PLOTTED AS A FUNCTION OF FREQUENCY, DISTANCE FROM THE CENTRAL RAY, AND THE ELECTRON-DENSITY SCALE FACTOR.

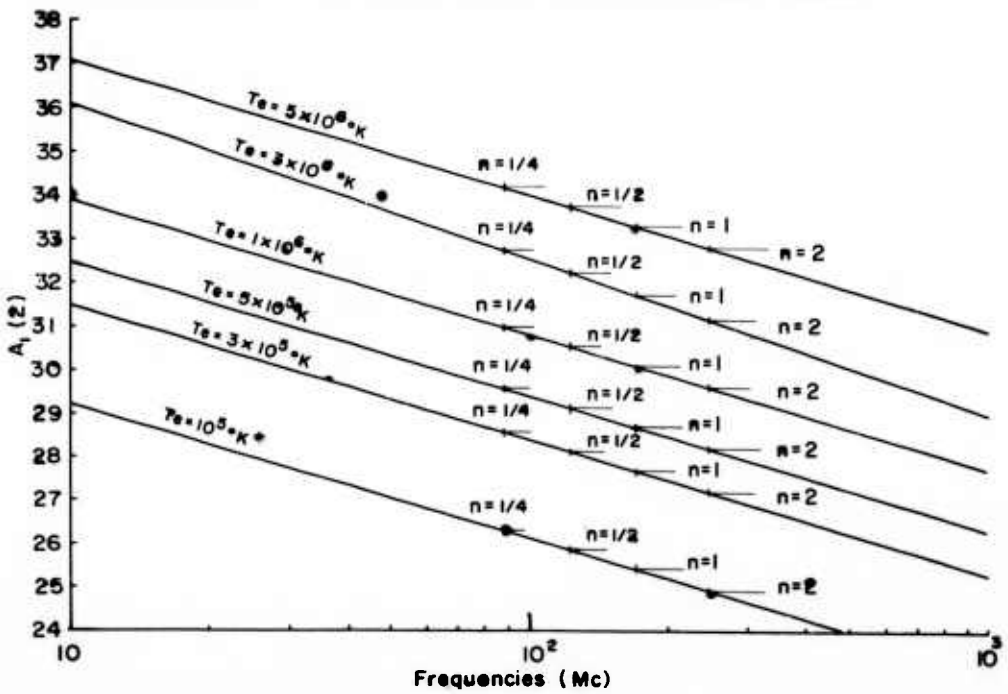

FIG. 3. SLOWLY VARYING FUNCTION $A_1(2)$ (SMERD) PLOTTED AS A FUNCTION OF FREQUENCY.

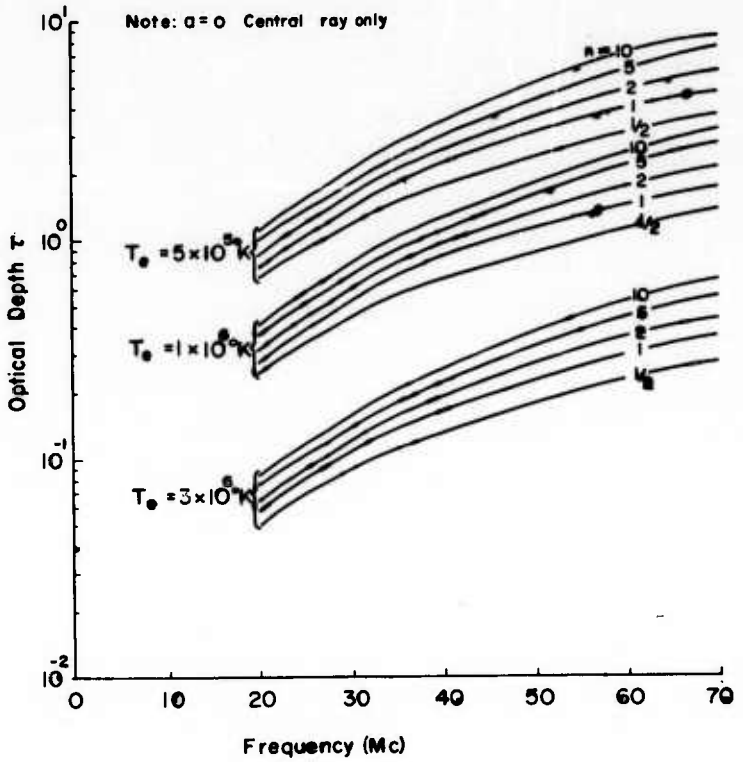

FIG. 4. OPTICAL DEPTH VS FREQUENCY.

$$\mu^2 = 1 - 12{,}400\ n\ f^{-2}\ \rho^{-6}\ (1 + 1.93\ \rho^{-10}), \qquad (10)$$

where f is in Mc and ρ is the distance from the sun's center in units of the solar photospheric radius (Fig. 5). When $\rho \gg 1$, we have the simpler form

$$\mu^2 = 1 - 12{,}400\ n\ f^{-2}\ \rho^{-6}. \qquad (11)$$

But the refractive index μ equals zero at the turning point for the central ray. Therefore, Eq. (11) reduces to

$$\rho_o = 4.8\, n^{1/6}\, f^{-1/3}. \tag{12}$$

With fixed n and f, ρ_o is thus determined. A set of curves of ρ_o for $n = 0.5, 1, 2, 5, 10$ and $f = 10$ to 80 Mc were plotted in Fig. 6. The plot for $n = 1$ agrees with Smerd's results [Ref. 7]. It also agrees with Jaeger's results in his Figure 2B [Ref. 8].

For other than the central ray, we need another important equation

$$\mu_a \rho_a = a \tag{13}$$

(For the derivation of Eq. (13) see Jaeger's paper [Ref. 8].) Therefore, Eq. (10) can be expressed as

$$1 - \frac{a^2}{\rho_a^2} - 12{,}400\, n\, f^{-2}\, \rho_a^{-6}\, (1 + 1.93\, \rho_a^{-10}) = 0. \tag{14}$$

For $\rho_a \gg 1$ we can simplify the above expression to

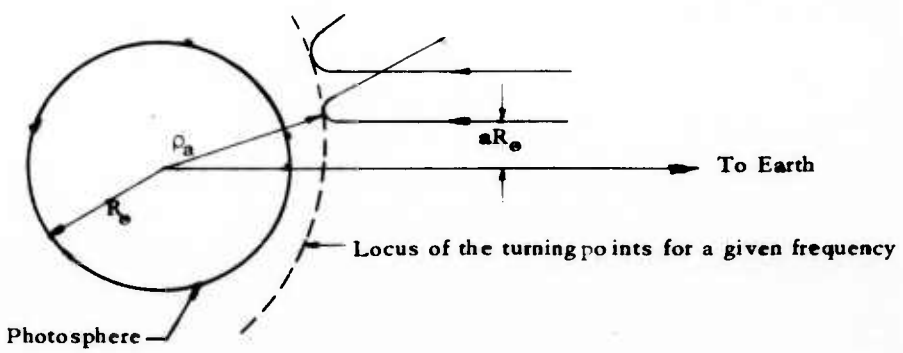

FIG. 5. TRAJECTORIES AND TURNING POINTS IN THE SOLAR CORONA

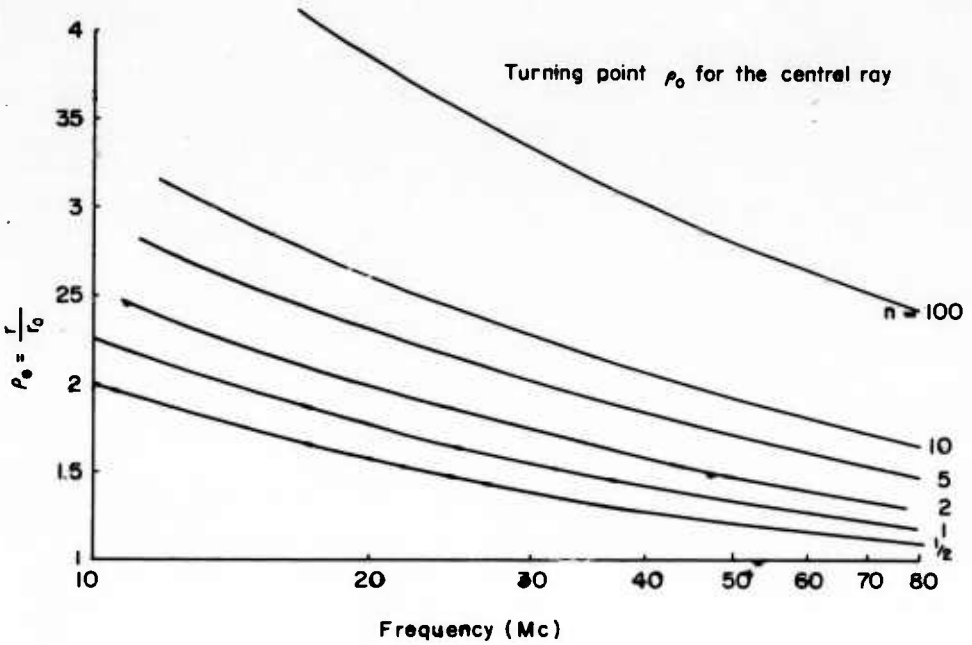

FIG. 6. CENTRAL-RAY TURNING POINT VS FREQUENCY.

$$\rho_a^6 - a^2\rho_a^4 - 12{,}400\ n\ f^{-2} = 0. \qquad (15)$$

For fixed n and f, the trajectories and loci of turning points can be determined. Jaeger [Ref. 8] has plotted various trajectories for f = 60 and 100 Mc.

C. RADAR CROSS SECTION, σ

Let W be the incident power per unit area on the sun. Then the power incident in a cylinder with radius $aR_\odot$ is $\pi a^2 R_\odot^2 W$. Let extreme rays of the thin cylinder, on returning to free space after refraction in the corona, form a cone of small semi-vertical angle $2\phi_a$ (solid angle $4\pi\phi_a^2$) (as in Fig. 1). Let the optical depth of each ray be 2τ, both inside and outside of the corona. Then the returning power W_1 per steradian is $e^{-2\tau}\ \pi a^2 R_\odot^2 W/4\pi\ \phi_a^2$. Hence the radar cross section σ is given by

$$\sigma = \frac{4\pi W_1}{W}$$

$$= e^{-2\tau} \pi a^2 R_\odot^2 / \phi_a^2$$

and
$$\frac{\sigma}{\pi R_\odot^2} = e^{-2\tau} \left(\frac{a}{\phi_a}\right)^2 \qquad (16)$$

for small values of a and ϕ_a. Strictly speaking, Eq. (16) should be expressed as

$$\frac{\sigma}{\pi R_\odot^2} = e^{-2\tau} \left(\frac{1}{d\phi_a/da}\right)^2 \qquad a = 0.$$

The relationship between ϕ_a and a is, for all a,

$$\phi_a = a \int_{\rho_a}^{\infty} \frac{d\rho}{\rho(n^2\rho^2 - a^2)^{1/2}} \qquad (17)$$

[Ref. 9]. If we calculated $d\phi_a/da$ at $a = 0$, we would have the value needed for ϕ_a/a in Eq. (16), in which ϕ_a and a are small quantities. The method of evaluating the integrand is given by Jeffreys and Jeffreys [Ref. 10].

The approximate answer for Eq. (17) is

$$\theta = h[3.77\ I(\rho_a + h) - 0.96\ I(\rho_a + 2h) + 1.12\ I(\rho_a + 3h)]$$

$$+ h \sum_{\rho_a + 4h}^{\rho_m} I(\rho) + \arcsin \frac{a}{\rho_m + \frac{1}{2}h}, \qquad (18)$$

where $I(\rho) = a\rho^{-1} (\mu^2\rho^2 - a^2)^{1/2}$. In the present calculation, $a = 0.1$, $h = 0.1$, and the first nine terms of $I(\rho_a + nh)$ were used, where $n = 1, 2, \ldots 9$. Figure 7 shows σ for various values of electron temperature, electron density multiplier n, and frequency.

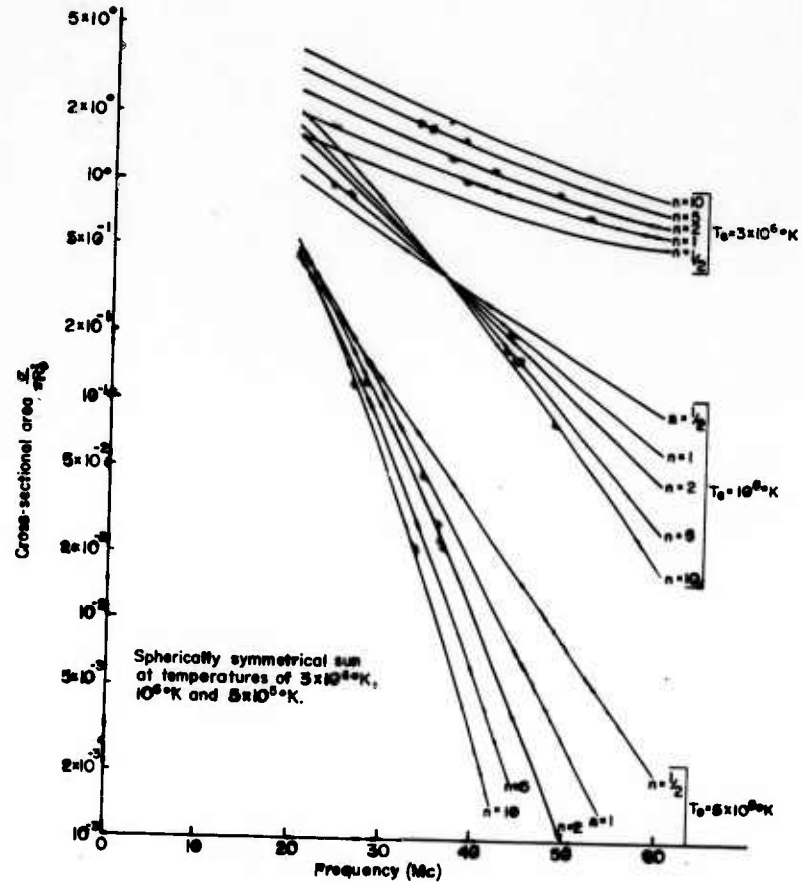

FIG. 7. CROSS-SECTIONAL AREA VS FREQUENCY.

D. SOLAR APPARENT TEMPERATURE, T_a

Three different concepts of temperature will be used. They are:

1. T_e, the electron kinetic temperature, generally called electron temperature in this report.
2. T_b, the brightness temperature, defined as the temperature of a black body which would yield a specific intensity I of thermal radiation equal to that observed, i.e., $I = B(T_b)$, and at radio frequencies $B(T_b)$ is suitably expressed by the Rayleigh-Jeans equation, $B(T) = 2kT/\lambda^2$.

3. T_a, the apparent temperature, defined as the mean brightness temperature with respect to the photospheric disk.

The characteristics of the radiation at a given frequency are specified by the brightness distribution over the disk. The brightness temperature, T_b, of a ray at emergence is given by

$$T_b = \int_0^{2\tau_\rho} T_e \, e^{-\tau} \, d\tau \tag{19}$$

[Ref. 3], where the integration is taken over the whole path of the ray through the solar atmosphere. The term τ is the optical depth measured back from emergence, and τ_ρ is its value at the turning point. The factor 2 in the upper limit is due to the symmetry of the trajectory about a radial vector through the turning point.

In the case of uniform temperature, the solution of the above integral of transfer for the ray emerging at a distance $aR_\odot$ from the central ray is

$$T_{b(a)} = T_e \left(1 - e^{-2\tau_{\rho a}}\right) \tag{20}$$

for rays whose turning points lie in the corona. For the distribution of τ_ρ and T_b with $T_e = 10^5$ K°, n = 1, and f = 18 Mc, see Figures 7 and 8 in the Bracewell and Preston paper [Ref. 9].

Assuming that the distribution of brightness temperature T_b has circular symmetry, then

$$T_a = 2\int_0^\infty T_{b(a)} \, a \, da. \tag{21}$$

Since the integrand of Eq. (21) is quite involved, a simplified method was used, as follows:

1. Calculate the values of $T_{b(a)}$ for different a, from a = 0 to a = 2.8, with fixed n, T_e, and f.

2. Plot the values of $T_{b(a)}$ versus a, as shown in Fig. 8.
3. Use graphical integration to calculate T_a.

$$T_{a1} = T_1 a_1^2$$

$$T_{a2} = T_2 (a_2^2 - a_1^2)$$

$$\vdots \qquad \vdots \qquad \vdots$$

$$T_{an} = T_n (a_n^2 - a_{n-1}^2), \text{ and}$$

$$T_a = \sum_{n=1}^{j} T_{an} \tag{22}$$

E. ECHO POWER INTERCEPTED BY THE RECEIVING ANTENNA, P_r

Stanford University and the Stanford Research Institute are preparing a new radar system for solar radar studies, and the MIT Lincoln Laboratory will also soon be studying the sun with a very large system in Texas. Characteristics of these systems are as follows:

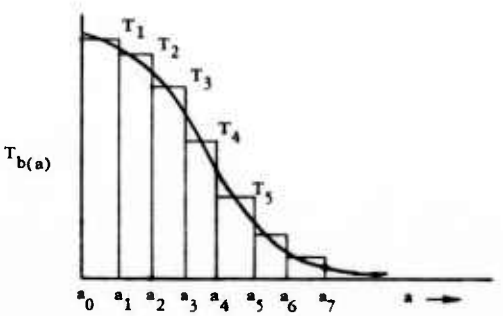

FIG. 8. BRIGHTNESS TEMPERATURE AS A FUNCTION OF DISTANCE FROM THE CENTRAL RAY.

1. STANFORD SYSTEM

Log-periodic antenna

Power averages 300 kw

Gain is approximately 25 db for frequencies from 20 to 60 Mc, independent of frequency

150-ft steerable parabolic-dish antenna

Power averages 300 kw

Aperture is πR^2, which is approximately 1650 m^2

(It is assumed, for the present, that this antenna is 100 percent efficient at all frequencies available from the transmitter--20 - 60 Mc).

These two systems have the same antenna gain at about 40 Mc. Thus, it is favorable to operate the 150 ft dish for frequencies higher than 40 Mc and to operate the log-periodic antenna for lower frequencies.

2. LINCOLN LABORATORY SYSTEM

Power averages 500 kw

Gain is approximately 35 db

This system is to be operated at a fixed frequency, 38 Mc.

If we assume that the pulse length exceeds the spread in delay time of the sun echo, we can use the standard radar equation,

$$P_r = \frac{P G_t}{4\pi R^2} \frac{1}{4\pi R^2} \frac{G_r \lambda^2}{4\pi} \sigma, \qquad (23)$$

where

P = radiated power in watts,

G_t = transmitting-antenna gain,

G_r = receiving-antenna gain,

σ = radar cross section of the sun, in square meters,

R = solar mean distance $\approx 1.49 \times 10^{11}$ meters, and

λ = wavelength in meters.

For a constant-aperture system, with the same antenna used for transmission and receiving, Eq. (23) could be rewritten as

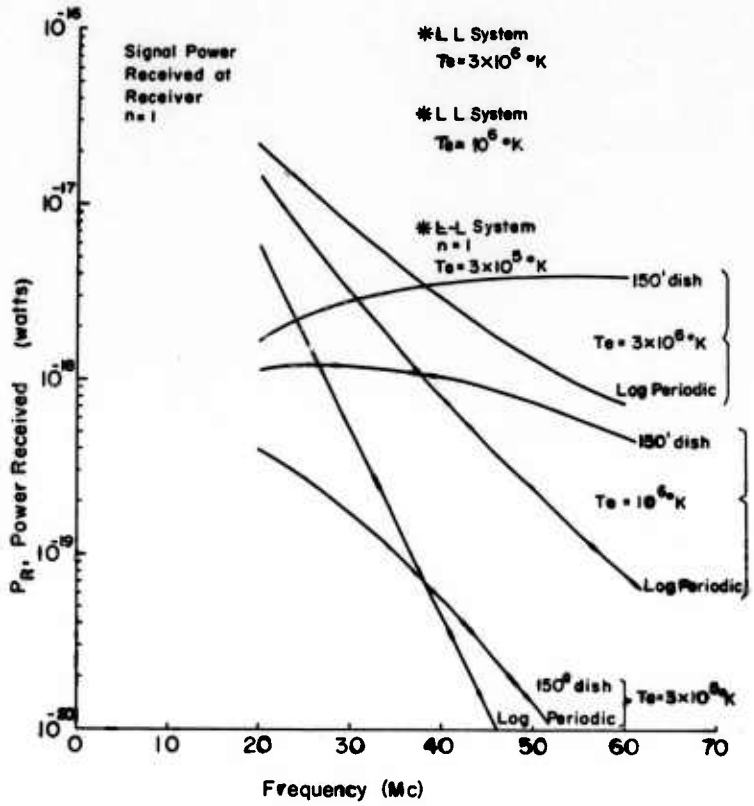

FIG. 9. SIGNAL POWER VS FREQUENCY.

$$P_r = \frac{P}{4\pi R^4} \frac{A^2}{\lambda^2} \sigma \,, \qquad (24)$$

where A = effective antenna area = $\frac{G\lambda^2}{4\pi}$. The values of P_r as a function of frequency for $n = 1$ and $T_e = 5 \times 10^5$, 10^6, and 3×10^6 °K are plotted in Fig. 9 for the systems under consideration.

F. GALACTIC NOISE, P_g

The equation for galactic noise is given by

$$P_g = 4 \times 10^{-21} \left(F + \frac{T_c}{T_o}\right) \text{ watts/cps.} \qquad (25)$$

[Ref. 11], where F = the receiver-noise factor, and

T_c/T_o = average galactic-noise factor $\approx 0.25\ \lambda^{2.3}$.

In the 20 to 60-Mc frequency band, $T_c/T_o \gg F$, and (25) reduces to

$$P_g = 10^{-21}\ \lambda^{2.3} \text{ watts/cps.} \qquad (26)$$

Under the assumption of uniform galactic-temperature distribution in the sky, all antennas see the same amount of galactic noise, since P_g is a function of operating frequency only. P_g is plotted in Fig. 10.

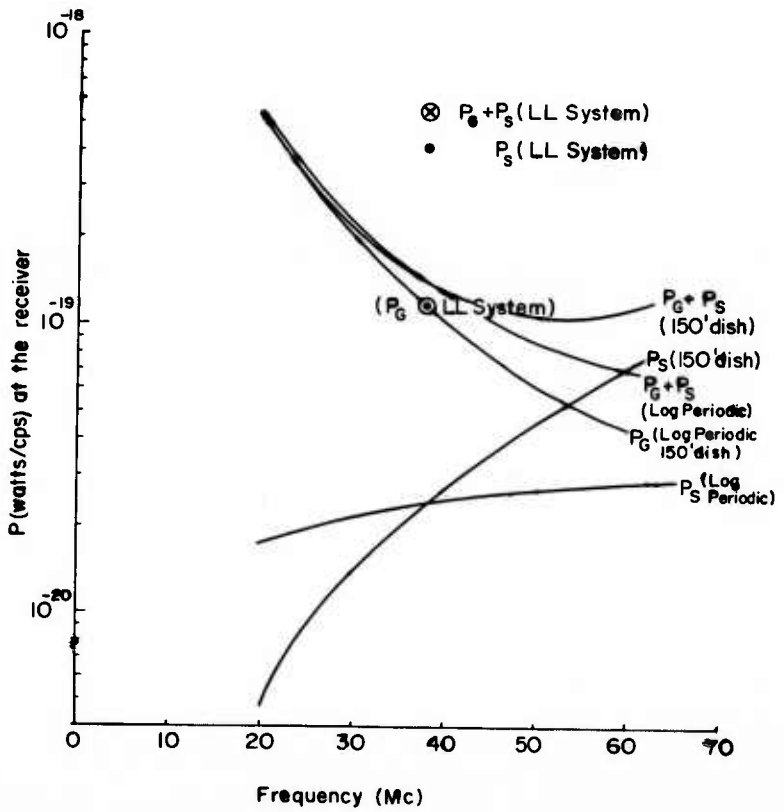

FIG. 10. GALACTIC AND SOLAR-NOISE POWER AT RECEIVER VS FREQUENCY.

G. SOLAR NOISE, P_s

The equation for P_s is given by

$$P_s = \frac{k\,T_a}{\lambda^2}\,\Omega_s\,\frac{\lambda^2\,G}{4\pi} \quad \text{watts/cps} \tag{27}$$

[Ref. 2] for the log-periodic antenna, and

$$P_s = k\,A\,\Omega_s\,\frac{T_a}{\lambda^2} \quad \text{watts/cps} \tag{28}$$

for the 150 - ft dish. In these expressions,

k = Boltzmann's constant
Ω_s = solid angle subtended by the sun's optical disk (steradian),
T_a = solar apparent temperature (see Sec. II-D),
A = antenna aperture in square meters, and
G = antenna gain.

From Eq. (27) and (28), we can see that P_s for the 150 -ft dish varies with respect to frequency much faster than P_s for the log-periodic antenna. The reasons are that

$P_s \propto T_a$ for the log-periodic antenna and

$P_s \propto T_a\,f^2$ for the 150 - ft dish.

Curves for P_s versus f are plotted in Fig. 10 for $n = 1$ and $T_e = 10^6$ °K.

H. BAND WIDTH, Δf

It is expected that the corona is rough, fluctuating, and rotating, so that the received echo will be spread in frequency. The center

frequency of the reflected signal will also be shifted relative to the transmitting frequency, because of the earth's orbital motion and rotation. This latter effect is of little concern here, since it can easily be computed and compensated for in the tuning of the receiver.

To a first approximation, we assume that the sphere seen at a particular operating frequency has a radius of ρ_o, where ρ_o is the distance of the turning point for a central ray from the center of the sun, and the rate of rotation of the corona is that of the solar photosphere. Thus the maximum band width is

$$\Delta f = \frac{2 \rho_o \omega_o}{c} f, \tag{29}$$

where

ω_o = the angular velocity of the sun at the equator
$\approx 2.7 \times 10^{-6}$ radians/sec

c = velocity of light, and

f = transmitting frequency in cps.

The values of ρ_o at various frequencies and values of n were obtained in Sec. II-B.

Curves for Δf versus f for $n = 1$ and 5 are plotted in Fig. 11. They are approximately linear, as the variation of ρ_o with respect to frequency is very close to linear (see Fig. 7).

I. SIGNAL-TO-NOISE RATIO, S/N

The signal-to-noise ratio is obtained from the above computed quantities from

$$S/N = \frac{P_r}{(P_s + P_g) \Delta f} . \tag{30}$$

Figures 12 and 13 were plotted for the systems mentioned above. In Fig. 12 there are two sets of curves; the solid lines represent $n = 1$ and $T_e = 10^6$ °K, and the dotted lines represent an extra 10 db of solar noise as an indication of the effect of non-quiet sun conditions.

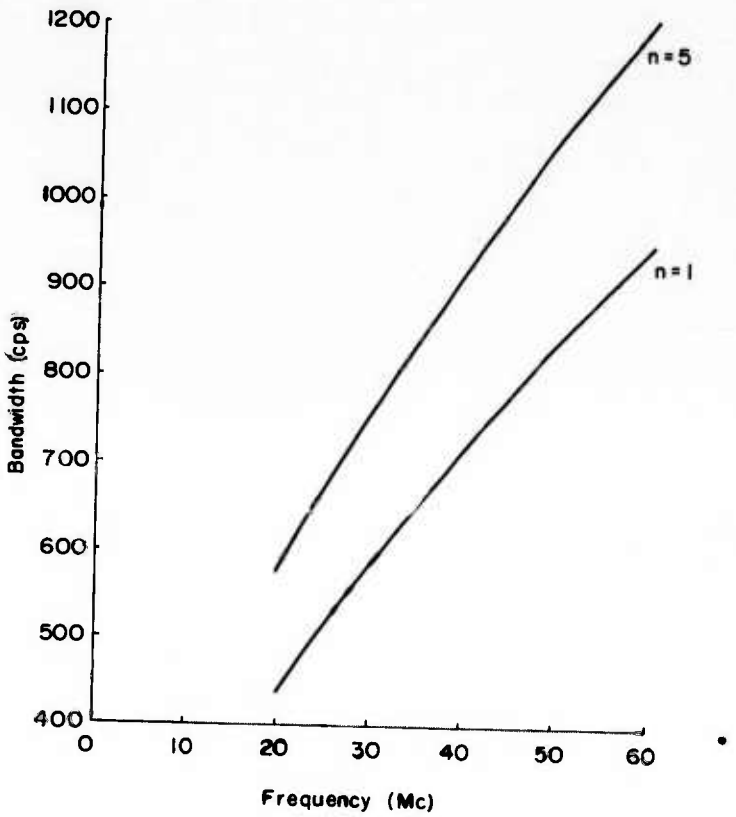

FIG. 11. BANDWIDTH VS FREQUENCY.

In Fig. 13 there are three sets of curves, representing three different electron temperatures--$T_e = 5 \times 10^5$, 10^6, and 3×10^6 °K--with n = 1 and 5. The general characteristics of the curves in Fig. 13 are:

1. The variation for S/N of the log-periodic antenna is almost linear with different T_e and n.
2. The S/N ratios for the two Stanford Antennas are equal at about 38 Mc. (Note that the noise is not entirely proportional to gain.) From Secs. II-F and II-G we have

$$P_s \propto T_a G,$$
$$P_g \propto 1/f^{2.3},$$

and total noise $P_N = P_s + P_g$.

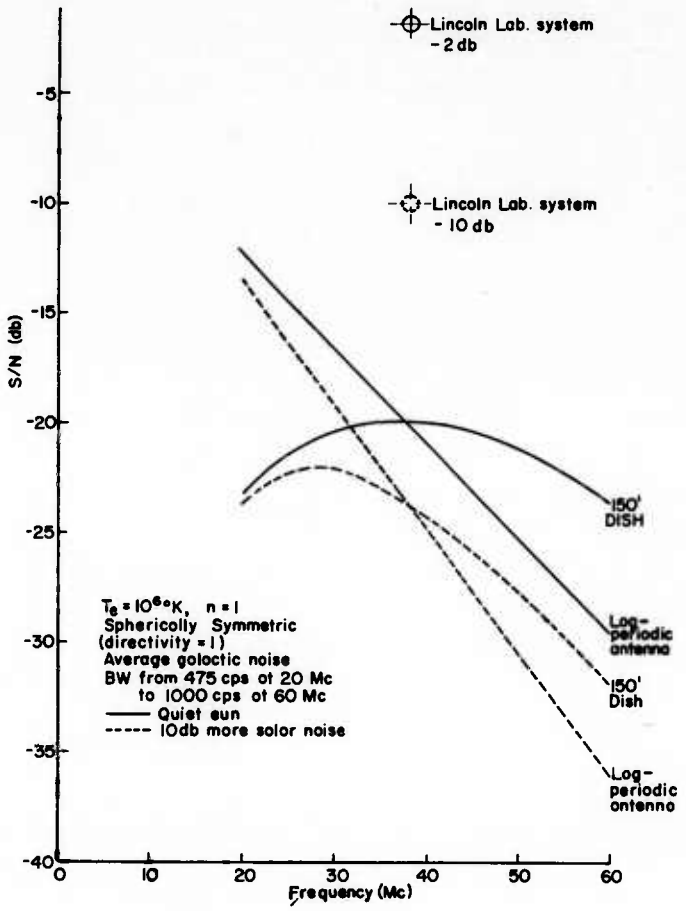

FIG. 12. S/N RATIO VS FREQUENCY, WITH SOLAR NOISE AS A PARAMETER.

3. The S/N is better for higher T_e. This effect is entirely due to the large radar cross section for higher T_e (see Sec. II-C). Although T_a increases for higher T_e, the rate of increase of cross section with respect to increasing electron temperature is greater than the rate of change of T_a (see Secs. II-C and II-D).
4. The change of n has little effect on S/N (see Secs. II-A and II-C).

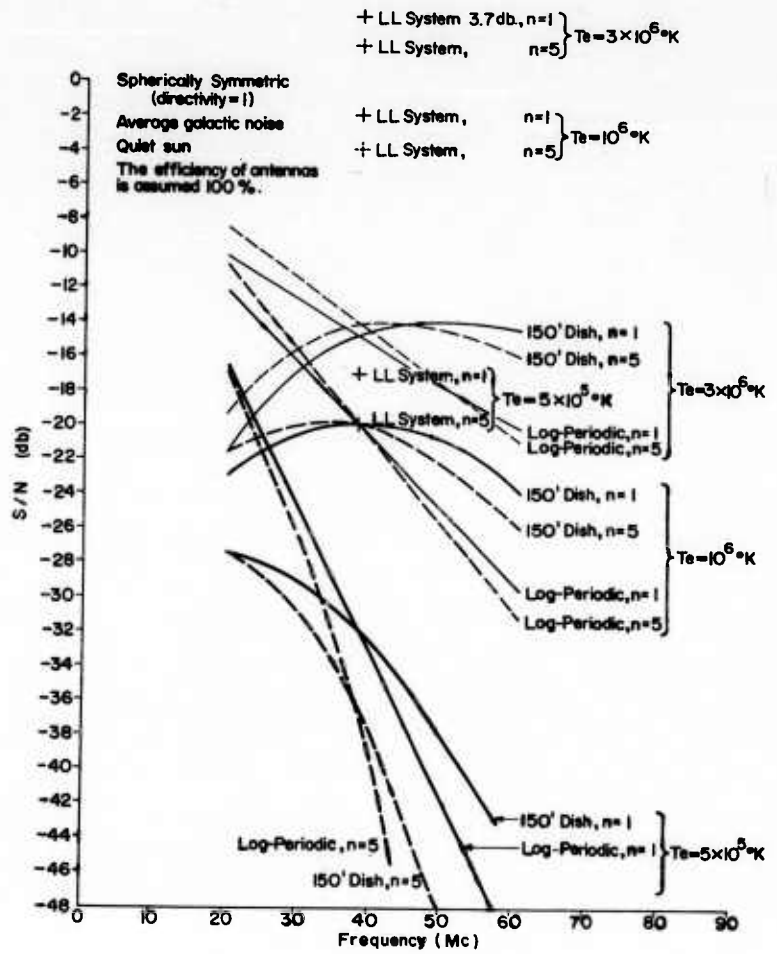

FIG. 13. S/N RATIO VS FREQUENCY, WITH ELECTRON TEMPERATURES AND DENSITIES AS PARAMETERS.

III. MAGNETIC FIELD EFFECT

In the presence of a magnetic field, the incident wave is split into two waves of equal strength, the ordinary and extraordinary waves.

The refractive index of the ordinary wave is the same as for the free-field case. The refractive index of the extraordinary wave is different; the zero refractive index of the extraordinary wave of the central ray is

$$x = 1 \pm y \qquad \text{for quasi-transverse} \tag{31}$$

$$x = 1 - y \qquad \text{for quasi-longitudinal} \tag{32}$$

where

$$x = \frac{f_o^2}{f^2},$$

$$y = \frac{f_h}{f}$$

$$f_o = \text{plasma-frequency} = \left(\frac{e^2 N}{4\pi^2 \epsilon_o m}\right)^{1/2},$$

$$f_h = \text{gyro-frequency} = \frac{eB}{2\pi m}, \text{ and}$$

f = wave frequency.

Assuming a magnetic dipole moment M at the center of the sun, the general magnetic field as a function of distance is

$$H(\rho) = \frac{M}{R_\odot^3 \rho^3} \tag{33}$$

$$H_o = \frac{M}{R_\odot^3}, \tag{34}$$

where H_o is the surface field at the equator. Then the gyro-frequency can be expressed as

$$f_h = \frac{e\mu\, H(\rho)}{2\pi m}.$$

Substituting f_o, f_h, and f into (31) and (32), we can express the distance of zero refractive level as

$$\rho_o = \left(\mp \frac{1.4\ H_o}{f} + \sqrt{\frac{1.96\ H_o^2 + 12{,}400}{f^2}} \right)^{1/3} \qquad \text{for quasi-transverse} \tag{35}$$

and

$$\rho_o = \left(\frac{1.4\ H_o}{f} + \sqrt{\frac{1.96\ H_o^2 + 12{,}400}{f^2}} \right)^{1/3} \qquad \text{for quasi-longitudinal} \tag{36}$$

where f is in Mc and $N = 10^{14}\ (1.55\ \rho^{-6})$. Hobbs [Ref. 12] used the quasi-transverse case associated with sunspots and found that the turning points for the extraordinary wave are further from the center of the sun than those for the ordinary wave. It is possible for the extraordinary wave to be reflected first and thus to suffer less absorption. If operating at a high frequency, say above 200 Mc, the returned signal is entirely from the extraordinary wave. The ordinary wave is almost totally absorbed before it reaches zero refractive-index level. In addition to the splitting effect, the general magnetic fields will also cause a differential in refraction and group velocity. These effects will depend on the strength of the field, the angular relationship between the wave normal and the direction of the field, and the electron density.

IV. CONCLUSION

The method of calculation in Section II indicates roughly the magnitude of the S/N which should be obtained with a solar radar system in a field-free case. For more accurate calculations of the S/N, it is advisable to use a computer. After more accurate experimental measurements have been made at several frequencies, it should be possible to improve very markedly our knowledge of such poorly known characteristics

as scale of roughness and motion in the corona, and the effects of local or general solar magnetic fields. The above computations help show the radar characteristics required for such measurements and the expected performance of several new solar radar systems.

A complementary approach to active radio studies of the sun is based on transmission through, instead of reflection from, the corona. Such studies are now being conducted, by utilizing the occultation of the Crab Nebula, but controlled radiations from space probes or radar reflections from planets near superior conjunction should provide even more information about the structure of the corona to tens of solar radii into the interplanetary medium [Ref. 13].

ACKNOWLEDGMENT

The author wishes to express his sincere appreciation to Professor V. R. Eshleman for his constant encouragement, guidance, and supervision. The author is also grateful to Mr. S. F. Smerd for his generosity in providing his as-yet-unpublished results.

This work was supported by the Electronics Research Directorate of the Air Force Cambridge Research Center, Bedford, Massachusetts, under contract AF 19 (604) 7436.

REFERENCES

1. V. R. Eshlemen, R. C. Barthle, and P. B. Gallagher, "Radar echoes from the sun", Science, 131, No. 3397, February 1960, pp. 329-332.

2. F. J. Kerr, "On the possibility of obtaining radar echoes from the sun and planets", Proc. IRE, 40, 6, June 1952, pp. 660-666.

3. G. P. Kuiper, The Sun, The University of Chicago Press, 1953, pp. 466-528.

4. S. F. Smerd and K. C. Westfold, "The characteristics of radio-frequency radiation in an ionized gas, with application to the transfer of radiation in the solar atmosphere", Phil. Mag., 40, 1949, pp. 831-848.

5. J. H. Chisholm, "Some physical aspects of radar probing of the sun's atmosphere", Notes of 1960 Summer Radar Astronomy Course at MIT.

6. S. F. Smerd, private communication.

7. S. F. Smerd, "A radio-frequency representation of the solar atmosphere", Proc. IEE (London), Part III, 97, November 1950, pp. 447-452.

8. J. C. Jaeger and K. C. Westfold, "Equivalent path and absorption for electromagnetic radiation in the solar corona", Aust. Journal of Sci. Re. A, 3, September 1950, pp. 376-386.

9. R. N. Bracewell and G. W. Preston, "Radio reflection and refraction phenomena in the high solar corona", The Astrophysical Journal, 123, 1, January 1956, pp. 14-29.

10. H. Jeffreys and B. S. Jeffreys, Methods of Mathematical Physics, Cambridge University Press, 1946, p. 264.

11. F. G. Bass and S. IA. Braude, "On the questions of reflecting radar signals from the sun", Ukrainian Journal of Physics, 2, 1957, pp. 149-163.

12. L. M. Hobbs, "Reflection of radio waves from the sun in the presence of the magnetic field of a sunspot", Research Report RS 12, Cornell University, July 1960.

13. V. R. Eshleman, P. B. Gallagher, and R. C. Barthle, "Theory of radar studies of the cislunar medium", Journal of Geophysical Research, 65, 10, October 1960, pp. 3079-3086.

DISTRIBUTION LIST
AF19(604)-7436

1 Air Force Missile Test Center
AFMTC Tech. Library - MU-135
Patrick Air Force Base
Florida

1 Air University Library
Maxwell Air Force Base
Florida

1 Aeronautical Systems Div.
(ASAPRL)
Wright-Patterson AFB
Ohio

1 Rome Air Development Center
(RCOIL-2)
Griffiss Air Force Base
New York

1 Air Force Missile Dev't Ctr.
(MDGRT)
Holloman Air Force Base
New Mexico

1 Air Force Office of Scientific
Research (SRY)
Washington 25, D. C.

1 Aeronautical Research Lab.
Technical Library
Building 450
Wright-Patterson Air Force Base
Ohio

1 Air Force Scientific Command
(SCAXC)
Andrews Air Force Base
Washington 25, D. C.

1 U.S. Army Signal Engr. Labs.
Technical Documents Center
Evans Signal Laboratory
Belmar, New Jersey

1 Chief of Res. and Dev't
Dept. of the Army
Washington 25, D. C.
Attn: Scientific Info. Br.

1 Commanding Officer
Diamond Ordnance Fuze Labs.
Washington 25, D. C.
Attn: ORDTL-012

1 Army Rocket And Guided
Missile Agency
Redstone Arsenal, Ala.
Attn: ORDXR-OTL, Tech. Lib.

1 Armed Services Tech. Info. Agcy.
1520 H. Street, N.W.
Washington 25, D. C.
Attn: Library

1 Director
Langley Research Center
National Aeronautics and Space
Administration
Langley Field, Virginia

10 Air Force Cambridge Res. Labs.
Office of Aerospace Research
(CRRELT)
L.G. Hanscom Field
Bedford, Massachusetts

2 Director, Avionics Div. (AV)
Bureau of Aeronautics
Dept. of the Navy
Washington 25, D.C.

2 Director (Code 2027)
U.S. Naval Research Lab.
Washington 25, D. C.

1 Director
U.S. Air Force Project RAnd
VIA: AF Liaison Office
The Rand Corporation
1700 Main Street
Santa Monica, Calif.

1 Boston Sub Office
Patent Prosecution Branch
(HQ. AMC)
Murphy General Hospital
Bldg. 133, 424 Trapelo Road
Waltham 54, Mass.

U.S. Army Aviation Human
Research Unit
U.S. Continental Army Command
P.O. Box 438
Fort Rucker, Alabama
1 Attn: Maj. Arne H. Eliasoon

Library
Boulder Laboratories
National Bureau of Standards
2 Boulder, Colorado

Institute of the Aeronautical
Sciences
2 East 64th Street
New York 21, New York
1 Attn: Librarian

Massachusetts Inst. of Tech.
Research Laboratory of Electr.
Building 26, Rm. 327
Cambridge 39, Mass.
1 Attn: John H. Hewitt

Electromagnetic Res. Corp.
5001 College Avenue
College Pk, Maryland
1 Attn: Mr. Martin Katzin

AVCO Research Laboratory
2385 Revere Beach Parkway
Everett 48, Massachusetts
1 Attn: Technical Librarian

The Mitre Corporation
244 Wood Street
Lexington 73, Massachusetts
1 Attn: Mrs. Jean E. Claflin,
Librarian

Wright Air Development Div.
Wright-Patterson Air Force Base
Ohio
1 Attn: Mr. Nicholas C. Draganjac
WWDBEG

Aeronautical Systems Div.
Wright-Patterson Air Force Base
1 Attn: Mr. Paul Springer
ASRNRE-3

Air Force Office of Scientific
Research (SRY)
Washington 25, D. C.
2 Attn: Mr. Wm. J. Otting

Rome Air Dev't Center
Griffiss Air Force Base
New York
1 Attn: Mr. Chas. A. Strom, Jr.

Wright Air Development Div.
Wright-Patterson Air Force Base
Ohio
1 Attn: Mr. Klaus Otten
(WCLNEL)

Aeronautical Systems Div.
Wright Patterson Air Force Base
Ohio
1 Attn: ASRNCE, Mr. Scheer

Headquarters, US Air Force
(AFOAC-S/E)
Washington 25, D.C.
1 Attn: Comm.-Elec. Directorate

Rome Air Development Ctr.
Griffiss Air Force Base
New York
1 Attn: Mr. Thomas G. Knight
(RCUELL)

Headquarters
United States Air Force
(AFDRD)
Washington 25, D. C.
1 Attn: Lt.Col. Wm. Hodson

Technical Advisory Committee
(Director of TeleComm. Systems)
Langley Air Force Base
1 Virginia

Office of Chief Signal Officer
U.S. Army Radio Frequency
Engineering Office
The Pentagon, Room BD 973
Washington 25, D. C.
1 Attn: Geo. W. Hayden, SIGFO-B4

Asst. Sec. of Defense for
Research and Dev't
Information Office Lib. Br.
Pentagon Bldg.
2 Washington 25, D. C.

U.S. Army Signal Radio Prop.
Agency
Ft. Monmouth, New Jersey
1 Attn: Mr. Fred. H. Dickson

Dept. of the Army
Evans Signal Lab.
Belmar, New Jersey
1 Attn: Alexander N. Beichek

U.S. Army Signal Engr. Labs.
Ft. Monmouth, New Jersey
1 Attn: Mr. Robt. Kulinyi
Long Range Radio Br.

Office of Science
Office of the Asst. Sec. of
Defense, Research and Engr.
1 Washington 25, D. C.

Federal Commun. Commission
Tech. Research Div.
Washington 25, D. C.
1 Attn: Mr. Harry Fine

Central Radio Prop. Lab.
National Bureau of Standards
Boulder, Colo.
1 Attn: K.A. Norton

Radio Commun. and Systm. Div.
85.00
Central Radio Propagation Lab.
National Bureau of Standards
Boulder, Colo
1 Attn: R. C. Kirby

U.S. Dept. of Commerce
National Bur. of Standards
Central Radio Prop. Lab.
Boulder, Colorado
1 Attn: Mr. George R. Sugar
Ionospheric Res. Sec.

U.S. Advisory Group
U.S. Embassy, The Hague
Dept. of State
Washington 25, D. C.
1 Attn: Mr. Pierre Bartholeme,
SADTC

Stanford Research Insti.
Menlo Park, California
1 Attn: Dr. D.R. Scheuch
Assistant Dir., Div. of
Engr. Research

Hughes Aircraft Company
Florence Ave. at Teale Street
Culver City, California
1 Attn: Documents Section
Research and Dev't
Library

Stanford Research Institute
Menlo Park, California
1 Attn: Dr. Allen M. Peterson

Melpar, Inc.
3000 Arlington Boulevard
Falls Church, Virginia
1 Attn: Mr.C.B. Raybuck
Vice-Pres. and Chief
Engineer

Raytheon Company
225 Crescent Street
Waltham, Massachusetts
1 Attn: Dr. D.A. Hedlund,
Communications and Data
Processing Operation

Bell Telephone Labs.
Murray Hill, New Jersey
1 Attn: Mr. K. Bullington

Collins Radio Company
855-35th Street, N.E.
Cedar Rapids, Iowa
1 Attn: Irvin H. Gerks

RCA Laboratories
David Sarnoff Research Ctr.
Princeton, New Jersey
1 Attn: Mr. Richard Jenkins

Pickard and Burns, Inc.
240 Highland Ave.
Needham 94, Massachusetts
1 Attn: Dr. Richard H. Woodward

Rand Corporation
1700 Main Street
Santa Monica, California
1 Attn: Edward E. Reinhart

General Electric Company
Defense Electrs. Division
735 State Street
Santa Barbara, California
1 Attn: Mr. Klaus G. Likehold,
Manager-Library

Ferranti-Packard Electric
Electronics Division
Industry Street
Toronto 15, Ontario, Canada
1 Attn: Mr. G.W.L. Davis

RCA Laboratories
Riverhead, Long Island
New York
1 Attn: Mr. Robt. Wagner

Air Force Cambridge Research
Laboratories
Office of Aerospace Research
L. G. Hanscom Field
Bedford, Mass.
1 Attn: CRRST, Mr. Leon Ames
9 Attn: CRRK, Mr. Wm. Griffin

Office of the Chief of Naval
Operations
Department of the Navy
Washington 25, D.C.
1 Attn: OP-583

Bureau of Ships, Code 819
Department of the Navy
Washington 25, D.C.
1 Attn: Mr.R.S. Baldwin

Librarian
U.S. Naval Postgraduate Sch.
1 Monterey, California

Chief of Naval Research
Electronics Br. (Code 427)
Department of the Navy
Washington 25, D.C.
2 Attn: Dr. Arnold Shostak

Commanding Officer and Dir.
U.S. Navy Electrs. Lab.
San Diego 52, California
1 Attn: D.P. Heritage
Head, Radio Branch

Commanding Officer
U.S. Naval Air Dev't Ctr.
Johnsville, Pennsylvania
1 Attn: NADC Library

Chief, Bureau of Ships
Dept. of the Navy
Washington 25, D.C.
2 Attn: 810

Chief, Bureau of Ordnance
Dept. of the Navy
Washington 25, D.C.
1 Attn: Code Rep-a

Commanding Officer and Dir.
U.S. Naval Electronics Lab
(Library)
1 San Diego 52, California

University of Florida
Electrical Engr. Dept.
Gainesville, Florida
1 Attn: Dr. George

Applied Physics Laboratory
Johns Hopkins University
8621 Georgia Avenue
2 Silver Spring, Maryland

The University of Michigan
Engineering Res. Institute
Willow Run Laboratories
Willow Run Airport
Ypsilanti, Michigan
1 Attn: Librarian

Cornell University
School of Electrical Engineering
Ithaca, New York
1 Attn: Dr. W. Gordon

Univ. of Texas
Electr. Engr. Research Lab.
Box 8026 University Station
Austin 12, Texas
1 Attn: Prof. A.W. Straiton

Georgia Technology Research
Institute
Engineering Experiment Station
722 Cherry Street, N.W.
Atlanta, Georgia
1 Attn: W.B. Wrigley, Head, Comm.
Branch

University of Illinois
Department of Physics
Urbana, Illinois
1 Attn: The Librarian

University of Tennesee
Department of Elec. Engineering
Knoxville, Tennessee
1 Attn: Prof. F.V. Schultz

Massachusetts Inst. of Tech.
Lincoln Laboratory
P.O. Box 73
Lexington 73, Massachusetts
1 Attn: Mr. J.H. Chisholm 6-357
1 Attn: Dr. Morton Loewenthal